NACA

RESEARCH MEMORANDUM

A FLIGHT INVESTIGATION TO DETERMINE THE EFFECTIVENESS OF MACH NUMBER 1.0, 1.2, AND 1.41 FUSELAGE INDENTATIONS FOR REDUCING THE PRESSURE DRAG OF A 45° SWEPTBACK WING CONFIGURATION AT TRANSONIC AND LOW SUPERSONIC SPEEDS

By Willard S. Blanchard, Jr., and Sherwood Hoffman

Langley Aeronautical Laboratory
Langley Field, Va.

NATIONAL ADVISORY COMMITTEE
FOR AERONAUTICS

WASHINGTON
May 16, 1957

NATIONAL ADVISORY COMMITTEE FOR AERONAUTICS

RESEARCH MEMORANDUM

A FLIGHT INVESTIGATION TO DETERMINE THE EFFECTIVENESS OF MACH NUMBER 1.0, 1.2, AND 1.41 FUSELAGE INDENTATIONS FOR REDUCING THE PRESSURE DRAG OF A 45° SWEPTBACK WING CONFIGURATION AT TRANSONIC AND LOW SUPERSONIC SPEEDS

By Willard S. Blanchard, Jr., and Sherwood Hoffman

SUMMARY

A flight investigation was conducted at zero lift to determine the effectiveness of three fuselage indentations for reducing the pressure drag of a 45° sweptback-wing—body configuration. The indentations investigated were designed for Mach numbers of 1.0, 1.2, and 1.41. The flight data were obtained for Mach numbers between 0.9 and 1.35 at corresponding Reynolds numbers of about 3.0×10^6 to 5.5×10^6 based on mean aerodynamic chord of the wing. The theoretical pressure drags were computed for each configuration by using the supersonic-area-rule theory and were compared with the experimental results.

The comparisons of the experimental and theoretical drags indicate that the supersonic area rule may be used to determine indentations having low pressure drag over a Mach number range in which the blunt leading edge is subsonic. Although the indentations were most effective in reducing the configuration drag at their respective design Mach numbers (compared with the drag of the other indentations), of the models tested, the Mach number 1.2 indentation gave the lowest average drag for the Mach number range investigated.

INTRODUCTION

In recent years considerable effort has been devoted to study of the range of applicability of the area-rule concept (refs. 1 and 2). One means of applying the area rule is by contouring or "indenting" the

fuselage so that the distribution of configuration cross-sectional area would be conducive to low drag. Normal or M = 1.0 indentations give large reductions in the sonic drag rise but generally become less efficient with increasing Mach number and eventually give unfavorable interference effects (ref. 3). Previous investigations show that indentations designed for Mach numbers up to 1.2 (refs. 4 and 5) and up to 1.4 (refs. 6 and 7) are more efficient than the Mach number 1.0 indentations at their design Mach numbers. Since the supersonic indentations have higher drag than the normal indentations at sonic speeds, the average drag over a Mach number range becomes important from a performance standpoint. Thus, it appears that for a desired Mach number range there is an optimum indentation that would yield the lowest average drag over this range.

The Langley Pilotless Aircraft Research Division has conducted a free-flight rocket-boosted model investigation of symmetrical fuselage indentations for a 45° swept wing having an aspect ratio of 4.0, a taper ratio of 0.6, and NACA 65A004 airfoil sections for design Mach numbers of 1.0, 1.2, and 1.41. The experimental results are compared with the theoretical pressure drag values determined from the supersonic-area-rule theory. The investigation covered a Mach number range from 0.9 to 1.35.

SYMBOLS

A cross-sectional area normal to body axis, sq in.

$A_n = \frac{2}{\pi}\int_0^{\pi} S'(x,\beta \cos\theta)\sin n\phi \, d\phi$

a acceleration, ft/sec^2

C_D total drag coefficient based on wing area

$C_{D,f}$ friction drag coefficient

ΔC_D pressure drag coefficient

$\bar{c}$ wing mean aerodynamic chord, 0.613 ft

g acceleration due to gravity, 32.2 ft/sec^2

l length of body, 3.33 ft

l_t total length of configuration projected along body axis, ft

[redacted]

M	free-stream Mach number
n	number of terms in the Fourier sine series
q	free-stream dynamic pressure, lb/sq ft
R	Reynolds number based on $\bar{c}$
r	fuselage radius, in.
S_w	wing area, leading and trailing edges extended to fuselage center line, sq ft
S_f	fuselage cross-sectional area, sq ft
S	total cross-sectional area, sq ft
$S' = dS/dx$	
W	weight, lb
x	distance measured from nose rearward along body axis
$\beta = \sqrt{M^2 - 1}$	
γ	elevation angle of flight path, deg
ϕ	Fourier angle $\cos^{-1}\left(1 - \frac{2x}{l_t}\right)$, deg
θ	roll angle, deg

MODELS

Physical dimensions of the models tested are presented in figures 1 to 3 and tables I and II. Figure 1 is a three-view drawing of the basic configuration. Figures 2 and 3 are dimensional fuselage-radius distribution and nondimensional total cross-sectional area distribution, respectively, of the four models tested. Tables I and II contain, respectively, airfoil ordinates and fuselage ordinates. Photographs of the models are presented as figure 4.

The basic configuration (model A) consisted of a 45° sweptback wing mounted on a parabolic body of fineness ratio 12.5. The wing had an aspect ratio of 4.0, a taper ratio of 0.6, and NACA 65A004 airfoil sections

parallel to the free-stream direction (root to tip). The configuration included swept, tapered, vertical stabilizing fins with thin double-wedge sections. The leading edge of the wing-body juncture was located at the 40-percent body station, which was also the station of maximum body diameter.

Models B, C, and D were identical to model A except that their fuselages were indented symmetrically for Mach numbers 1.0, 1.2, and 1.41, respectively. As is stated in reference 2, for radially symmetrical modifications, the area used for the optimum indentation is obtained by averaging the frontal projection of wing areas cut by Mach planes at all angles of roll θ of the Mach planes with respect to the configuration. These average indentations were obtained by using Faget's rapid "method of hoops" (ref. 6). The frontal projection of the average area distribution of each indented configuration at its design Mach number corresponded to the normal cross-sectional area distribution of the basic parabolic fuselage. No area adjustments were made for the thin stabilizing fins of the models.

TEST TECHNIQUE

The models were flight tested at the Langley Pilotless Aircraft Research Station at Wallops Island, Va. All four models were launched from a rail launcher. Figure 4(e) is a photograph of one of the model-booster combinations in the launching position. Each model was boosted to its peak Mach number by a solid-fuel rocket motor 5 inches in diameter and 65 inches long. Each model was tandem-mounted ahead of its booster, as is shown in figure 4(e). The model-booster juncture for each model was a free-sliding fit so that, at burnout of the booster rocket fuel, the higher drag-weight ratio of the booster, as compared with that of the model, allowed the model to separate longitudinally from the booster. At the time of separation the small rectangular fins located near the forward end of the booster motor were mechanically deflected. This fin deflection in turn served to deflect the flight path of the booster motor away from the model flight path; thus, the line of sight between the model and the ground-based radar units was left clear in order to simplify the job of tracking the model and to improve the quality of the radar data.

All data were recorded during coasting flight as the models, free from their boosters, decelerated through the Mach number range reported in this paper. The models were tracked in flight by a CW Doppler radar unit to obtain velocity data and by a modified SCR 584 radar unit to obtain flight-path data. Immediately after each flight, atmospheric conditions, including winds aloft, were measured with rawinsonde equipment which transmitted this information to a ground receiving station while being carried aloft by a weather balloon.

DATA REDUCTION AND ANALYSIS

The total drag coefficient was evaluated by using the expression

$$C_D = \frac{-W}{gqS_w}(a + g \sin \gamma)$$

where a was obtained by differentiating the velocity-time curve obtained from Doppler radar.

The probable error in the total drag coefficient was estimated to be less than ±0.0007 at supersonic speeds and ±0.001 at subsonic speeds. The Mach numbers were determined within ±0.01 throughout the test range.

Pressure drag coefficient was obtained from

$$\Delta C_D = C_D - C_{D,f}$$

where $C_{D,f}$ was calculated for the basic configuration by using Van Driest's flat-plate skin-friction coefficients from reference 8 for the Reynolds numbers of the test range. Flow over the body was assumed to be turbulent. Flow over the smooth metal wings and tails was assumed to be laminar to the 40- and 50-percent-chord stations, respectively. The computed value of friction drag coefficient thus obtained was 0.010 at $M = 0.9$. Since within the accuracy of the data this value agrees with the total drag coefficient of each of the models at $M = 0.9$, the friction-drag level was adjusted to exactly equal the total drag coefficient of each model at $M = 0.9$ in order to facilitate comparison of the pressure drag coefficients. Test results from reference 9 and unpublished data have shown that, for fuselage afterbodies like those used in these tests, the subsonic base drag is approximately zero and is so nearly constant throughout the Mach number range that it could be neglected when the data are analyzed. Reference 9 also shows that the fin drag rise is negligible.

The theoretical pressure drags of the wing-body combinations were calculated by using the supersonic area rule of reference 2. The computational procedure is described in references 5 and 10. Since the models were symmetrical, only the frontal projection of the oblique areas cut by inclined Mach planes between roll angles of 0° and 90° had to be considered. These corresponded to values of $\beta \cos \theta$ equal to 0, 0.2, 0.4, 0.6, and 0.8. It should be noted that for $\theta = 0^\circ$ the Mach planes are perpendicular to the wing plane and are inclined at the Mach angle from the axis of symmetry. Since all the fuselages were slender (fineness ratio 12.5), it was possible to simplify the work by using the normal

area distribution of the fuselages in combination with the oblique area distributions of the wings. It has also been assumed, for the calculations, that a cylinder can be added to the base of the body without altering the pressure drag. If this were not done, the solution would require the flow to fill the area behind the base; this condition would exceed the limitations of the linearized theory. All the area distributions and their slopes were obtained graphically (see ref. 11). The computed drags were for the condition of a subsonic leading edge for the wing. The Fourier sine series used for calculating the pressure drag was evaluated for 33 harmonics by using the expression

$$\Delta C_D = \frac{1}{2S_w}\int_0^{\pi/2}\sum_{n=1}^{33} nA_n^2 d\theta$$

RESULTS AND DISCUSSION

Reynolds numbers for the four models tested, based on mean aerodynamic chord of the wing, varied from about 3×10^6 at $M = 0.9$ to approximately 5.5×10^6 at $M = 1.35$, as shown in figure 5.

Total Drag

The variations with Mach number of the measured total drag coefficients and the adjusted friction drag coefficients are shown in figure 6. Total drag coefficients from figure 6 are shown plotted on common axes in figure 7 to facilitate direct comparison. The comparison shows the following significant results: (1) the basic configuration (model A) has slightly lower drag at $M = 0.9$, but at Mach numbers above 1.13 its drag is higher than that of the other three models tested; (2) model B (Mach number 1.0 indentation) has the lowest total drag at Mach numbers between 0.97 and 1.11; (3) model C (Mach number 1.2 indentation) has the lowest total drag between $M = 1.11$ and $M = 1.31$; and (4) the trend of the total drag coefficient curves indicates that the Mach number 1.41 indentation (model D) yields the lowest total drag at Mach numbers greater than 1.31. It should be remembered that, as mentioned earlier in the paper, the fuselages of models B, C, and D each had 18 percent less volume than the fuselage of model A, as a result of the area-rule indentations.

Pressure Drag

Figure 8 shows some typical slope distributions and some typical values of theoretical pressure drag coefficient computed by using the Fourier sine series solution. In figure 8(a), the nondimensional area-distribution slope of model B is shown plotted against Fourier angle ϕ at values of $\beta \cos \theta = 0$ and 0.8. Figure 8(b) shows, also for model B, values of pressure drag coefficient computed for values of $\beta \cos \theta$ between 0 and 0.8 and for values of n (number of terms in the Fourier sine series) from 1 to 33. Note, in figure 8(b), that the Fourier sine series apparently approaches convergence at much lower values of n for $\beta \cos \theta = 0$ than for $\beta \cos \theta = 0.8$. This convergence may be expected from a comparison of slopes of the area distributions corresponding to $\beta \cos \theta = 0$ and to $\beta \cos \theta = 0.8$ (as seen in fig. 8(a)). For $\beta \cos \theta = 0$, the curve is relatively smooth and thus, the first few terms of the Fourier series are allowed to approach convergence closely (fig. 8(b)). For $\beta \cos \theta = 0.8$, the curve has a number of inflections and sharp peaks and the series therefore converges more slowly.

Shown in figure 9 are experimental and theoretical values of pressure drag coefficients. Inasmuch as the subsonic drag levels were about the same for the four models tested, the experimental values of pressure drag shown in figure 9(a) have about the same relationship with one another as the experimental values of total drag shown in figures 6 and 7. In terms of pressure drag, however, it may now be noted (fig. 9(a)) that, at $M = 1.0$, model B ($M = 1.0$ indentation) had 50-percent less pressure drag than model A (basic configuration); at $M = 1.2$, model C ($M = 1.20$ indentation) had about 40 percent less. Trends of the data indicate that, at $M = 1.4$, model D ($M = 1.41$ indentation) would have about 20-percent less pressure drag than model A. Thus, in view of the lesser (by 18 percent) fuselage volumes of models B, C, and D, with respect to model A, it appears that, at their design Mach numbers, the $M = 1.0$ and the $M = 1.2$ indentations had considerably less pressure drag than the basic configuration. On the same basis the $M = 1.41$ indentation does not appear to show near its design Mach number any appreciable drag advantage over the basic configuration. It is apparent from figure 9(a) that, for Mach numbers between 0.9 and 1.3, the $M = 1.20$ indentation yields the lowest average pressure drag of the four configurations tested. Theory predicts that, at their design Mach numbers, the $M = 1.0$ indentation and the $M = 1.2$ indentation would have about 40 percent less pressure drag than the basic configuration as shown in figure 9(b).

The upper limit for the calculations was selected arbitrarily at $\beta \cos \theta = 0.8$. This corresponds to $M = 1.28$ at zero roll angle. At higher Mach numbers the Mach lines approach the sweepback of the blunt leading edge of the wing where the linearized assumptions of the theory would no longer apply. Although a direct comparison of the theoretical and measured ΔC_D was not obtained for model D at its design Mach number

of 1.41, the theoretical trends are in agreement with the experimental results over most of the Mach number range. The relatively high pressure drag of the $M = 1.41$ indentation near $M = 1.0$ may be explained by the relatively large slopes of its normal cross-sectional area distribution as shown in figure 3. Conversely, the relatively small slopes of the area distribution of the $M = 1.0$ indentation explain its comparatively low pressure drag at $M = 1.0$.

Shown in figure 10 are direct comparisons of experimental and theoretical pressure drag coefficients for each of the four models tested. For models A and B the theoretical values average about $0.002\Delta C_D$ lower than the measured values at low supersonic speeds. This deviation is not unusual for area-rule computations since discrepancies of the same order of magnitude have been reported for sweptback wings in references 4 and 10. For models C and D, theory more nearly predicts the pressure drag throughout the Mach number range reported. The area distributions of these models were more nearly smooth at the higher Mach numbers than were those of models A and B. It follows that the Fourier sine series solution would converge more rapidly and give better agreement with the test results for models C and D at the higher speeds.

In a previous investigation (ref. 7) conducted in the Langley 8-foot transonic pressure tunnel, tests of configurations similar to those of this investigation indicated results that agree closely with those reported herein. The models of reference 7 differed from those of this test in that the wings were cambered, had 0.15 taper, and had a spanwise variation of thickness ratio. In general, it appears that, for sweptback wing-body configurations, the supersonic area rule may be used to calculate indentations which yield low drag at predetermined Mach numbers. Furthermore, it appears that the Fourier sine series solution will predict indentations for low average drag over a Mach number range.

CONCLUDING REMARKS

A zero-lift free-flight drag investigation was conducted to determine the effectiveness of three fuselage indentations for reducing the pressure drag of a 45° sweptback wing-body configuration. The indentations investigated were designed for Mach numbers of 1.0, 1.2, and 1.41. The flight data were obtained for Mach numbers between 0.9 and 1.35 with corresponding Reynolds numbers from about 3.0×10^6 to 5.5×10^6 based on wing mean aerodynamic chord. The theoretical pressure drags of the configurations were computed by using supersonic-area-rule theory for comparison with the experimental results.

[redacted]

The experimental and theoretical drag comparisons indicate that the supersonic area rule may be used to determine indentations having low pressure drag for a range of Mach number in which the blunt leading edge of the sweptback wing is subsonic. Although the indentations were most effective in reducing the configuration drag at their respective design Mach numbers (in comparison with the drags of the other indentations), of the configurations tested, the Mach number 1.2 indentation gave the lowest average drag for the Mach number range investigated.

Langley Aeronautical Laboratory,
National Advisory Committee for Aeronautics,
Langley Field, Va., February 18, 1957.

REFERENCES

1. Whitcomb, Richard T.: A Study of the Zero-Lift Drag-Rise Characteristics of Wing-Body Combinations Near the Speed of Sound. NACA Rep. 1273, 1956. (Supersedes NACA RM L52H08)

2. Jones, Robert T.: Theory of Wing-Body Drag at Supersonic Speeds. NACA RM A53H18a, 1953.

3. Hoffman, Sherwood: A Flight Investigation of the Transonic Area Rule for a 52.5° Sweptback Wing-Body Configuration at Mach Numbers Between 0.8 and 1.6. NACA RM L54H13a, 1954.

4. Holdaway, George H., and Hatfield, Elaine W.: Investigation of Symmetrical Body Indentations Designed to Reduce the Transonic Zero-Lift Wave Drag of a 45° Swept Wing With an NACA 64A006 Section and With a Thickened Leading-Edge Section. NACA RM A56K26, 1957.

5. Holdaway, George H.: Comparison of Theoretical and Experimental Zero-Lift Drag-Rise Characteristics of Wing-Body-Tail Configurations Near the Speed of Sound. NACA RM A53H17, 1953.

6. Hoffman, Sherwood, Wolff, Austin L., and Faget, Maxime A.: Flight Investigation of the Supersonic Area Rule for a Straight Wing-Body Configuration at Mach Numbers Between 0.8 and 1.5. NACA RM L55C09, 1955.

7. Loving, Donald L.: A Transonic Investigation of Changing Indentation Design Mach Number on the Aerodynamic Characteristics of a 45° Sweptback-Wing—Body Combination Designed for High Performance. NACA RM L55J07, 1956.

8. Van Driest, E. R.: Turbulent Boundary Layer in Compressible Fluids. Jour. Aero. Sci., vol. 18, no. 3, Mar. 1951, pp. 145-160, 216.

9. Morrow, John D., and Nelson, Robert L.: Large-Scale Flight Measurements of Zero-Lift Drag of 10 Wing-Body Configurations at Mach Numbers From 0.8 to 1.6. NACA RM L52D18a, 1953.

10. Alksne, Alberta: A Comparison of Two Methods for Computing the Wave Drag of Wing-Body Configurations. NACA RM A55A06a, 1955.

11. Nelson, Robert L., and Welsh, Clement J.: Some Examples of the Applications of the Transonic and Supersonic Area Rules to the Prediction of Wave Drag. NACA RM L56D11, 1956.

[redacted]

TABLE I.- COORDINATES OF NACA 65A004 AIRFOIL SECTION

[Stations measured from leading edge]

Station, percent chord	Ordinate, percent chord
0	0
.5	.311
.75	.378
1.25	.481
2.5	.656
5.0	.877
7.5	1.062
10	1.216
15	1.463
20	1.649
25	1.790
30	1.894
35	1.962
40	1.996
45	1.996
50	1.952
55	1.867
60	1.742
65	1.584
70	1.400
75	1.193
80	.966
85	.728
90	.490
95	.249
100	.009
L.E. radius: 0.102 percent chord T.E. radius: 0.010 percent chord	

TABLE II.- BODY COORDINATES

[Stations measured from body nose]

Station, in.	Fuselage ordinates, in.			
	Model A	Model B	Model C	Model C
0	0	0	0	0
1	.194	.194	.194	.194
2	.375	.375	.375	.375
3	.544	.544	.544	.544
4	.700	.700	.700	.700
5	.844	.844	.844	.844
6	.975	.975	.975	.975
7	1.094	1.094	1.094	1.094
8	1.200	1.200	1.200	1.200
9	1.296	1.296	1.296	1.296
10	1.375	1.375	1.375	1.375
11	1.444	1.444	1.444	1.444
12	1.500	1.500	1.500	1.500
13	1.544	1.544	1.544	1.544
14	1.575	1.575	1.575	1.575
15	1.594	1.594	1.594	1.594
16	1.600	1.600	1.577	1.500
17	1.599	1.572	1.527	1.414
18	1.594	1.502	1.449	1.332
19	1.588	1.422	1.354	1.259
20	1.578	1.328	1.259	1.214
21	1.565	1.230	1.165	1.222
22	1.550	1.155	1.120	1.245
23	1.532	1.102	1.138	1.272
24	1.511	1.086	1.178	1.293
25	1.488	1.091	1.214	1.293
26	1.461	1.088	1.232	1.285
27	1.432	1.081	1.237	1.271
28	1.400	1.071	1.231	1.252
29	1.365	1.056	1.209	1.228
30	1.328	1.047	1.185	1.202
31	1.288	1.074	1.160	1.170
32	1.244	1.107	1.120	1.135
33	1.199	1.135	1.092	1.097
34	1.150	1.134	1.053	1.054
35	1.099	1.099	1.010	1.007
36	1.044	1.044	.961	.957
37	.988	.988	.913	.904
38	.928	.928	.861	.847
39	.865	.865	.810	.788
40	.800	.800	.760	.730

[redacted]

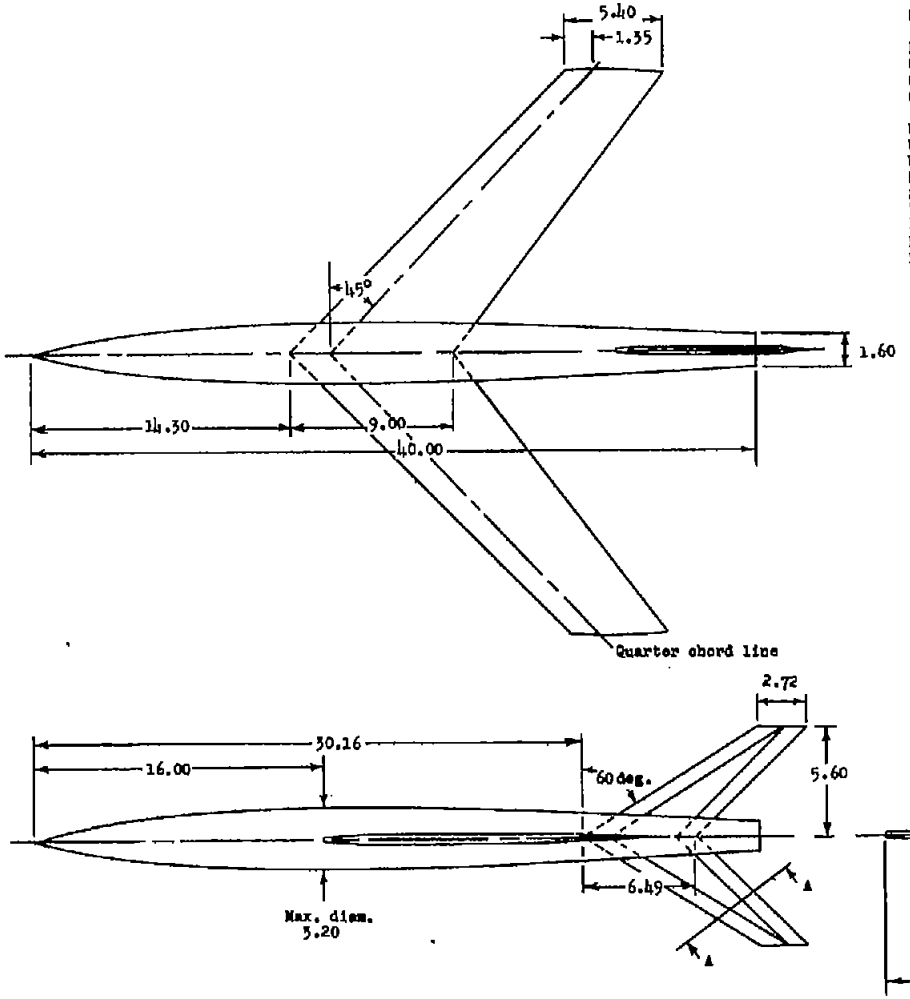

Model Characteristics

Basic configuration	Model A
Configuration with M = 1.0 indentation	Model B
Configuration with M = 1.2 indentation	Model C
Configuration with M = 1.41 indentation	Model D
Wing aspect ratio	4.0
Wing taper ratio	0.6
Wing mean aerodynamic chord, ft	0.613
Free-stream airfoil	NACA 65A004
Sweepback angle of quarter chord, deg	45
Total wing plan-form area, sq ft	1.440
Exposed fin plan-form area, sq ft	0.259
Body fineness ratio	12.5
Body frontal area, sq ft	0.056

Figure 1.- Details and dimensions of basic configuration. All dimensions are in inches.

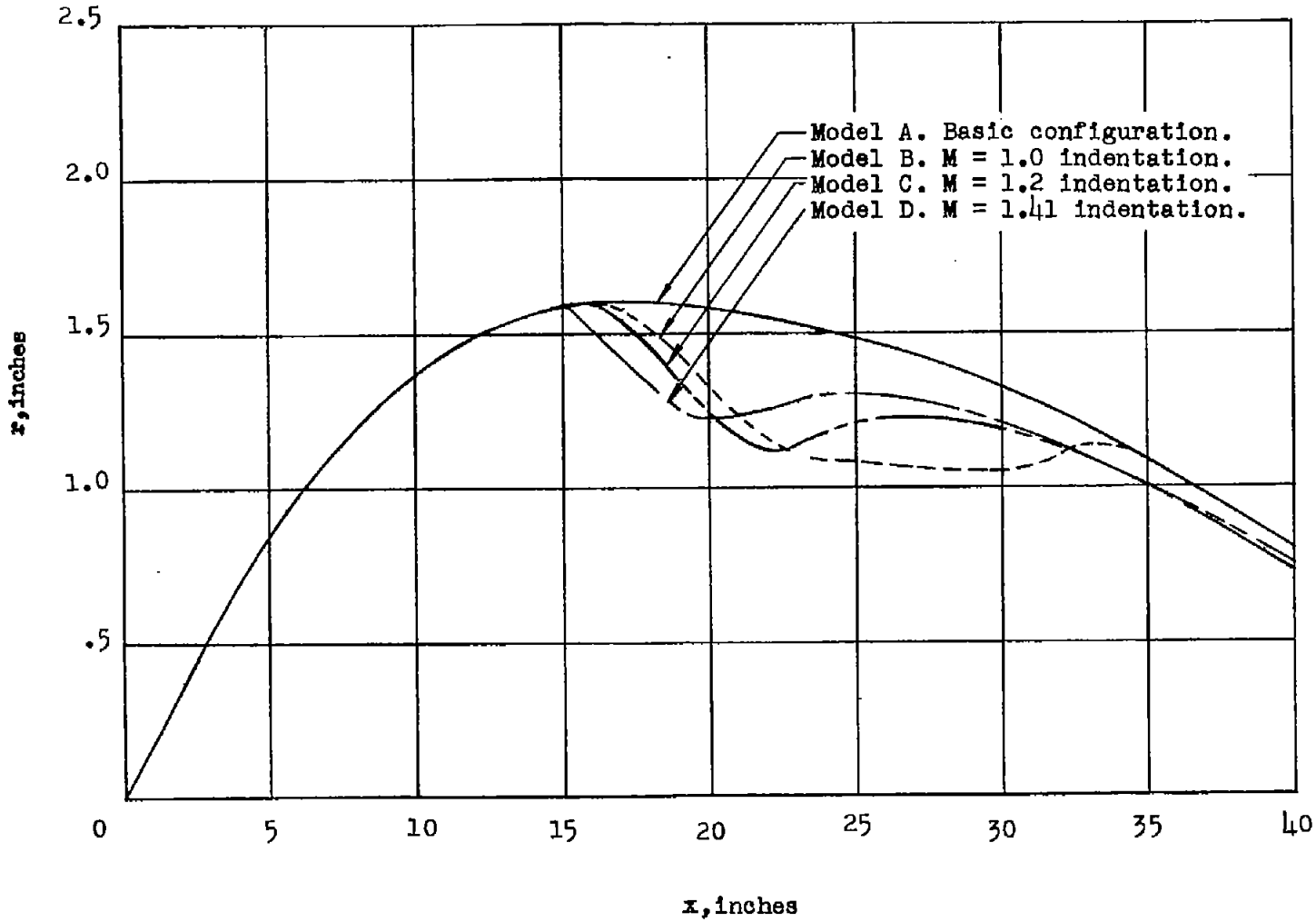

Figure 2.- Radius distribution of the fuselages tested.

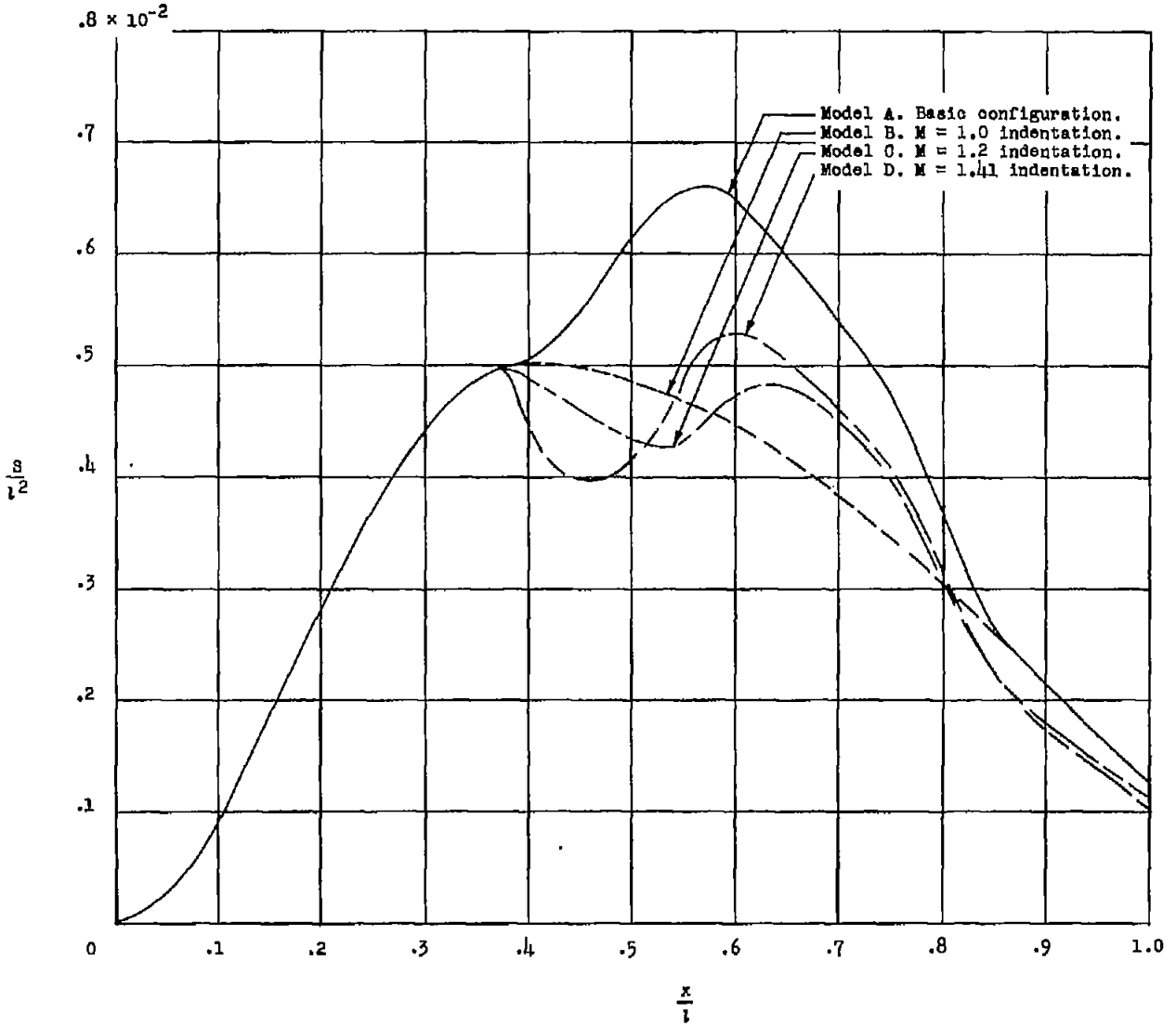

Figure 3.- Normal cross-sectional area distributions of models tested.

(a) Model A; basic configuration. L-92589.1

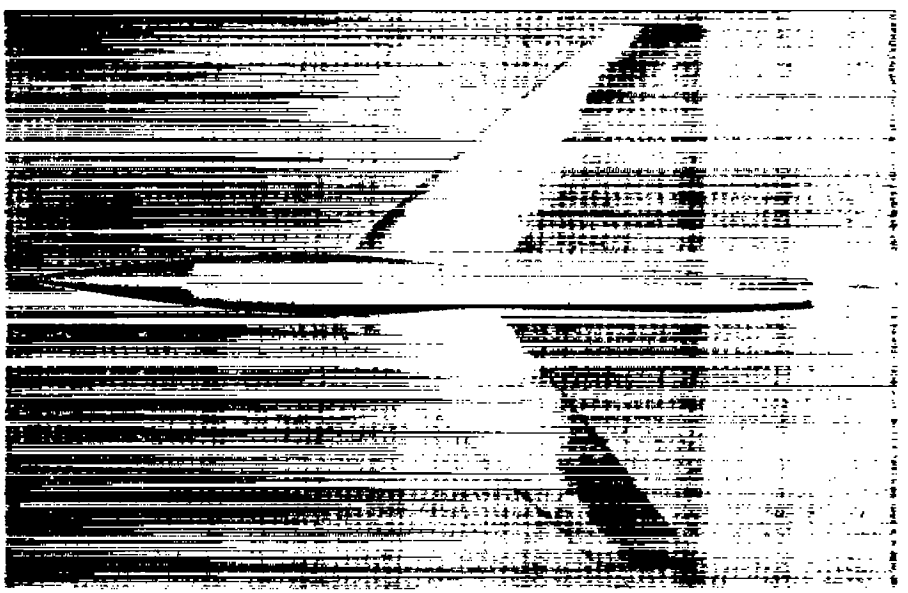

(b) Model B; M = 1.0 indentation. L-92590.1

Figure 4.- Photographs of models tested.

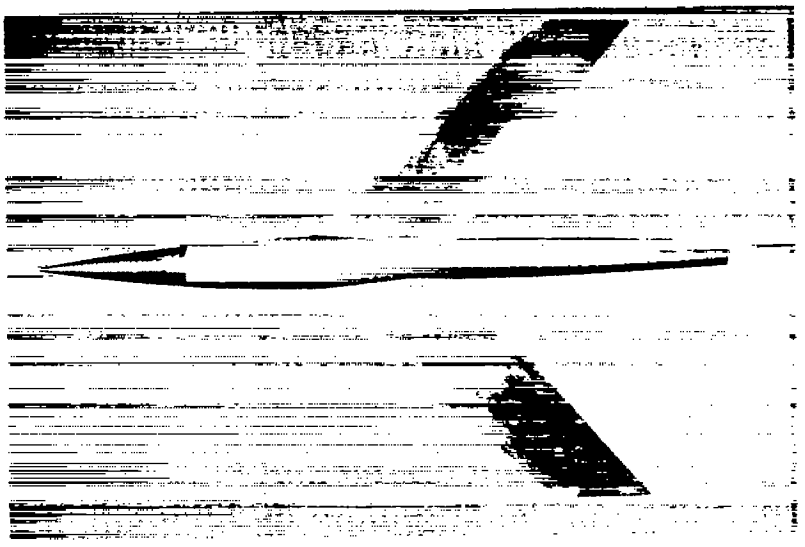

(c) Model C; M = 1.2 indentation. L-92208.1

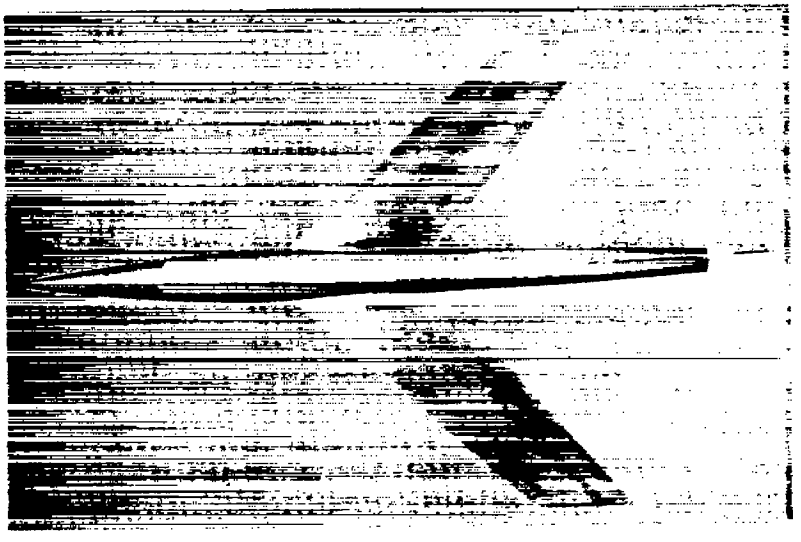

(d) Model D; M = 1.41 indentation. L-92210.1

Figure 4.- Continued.

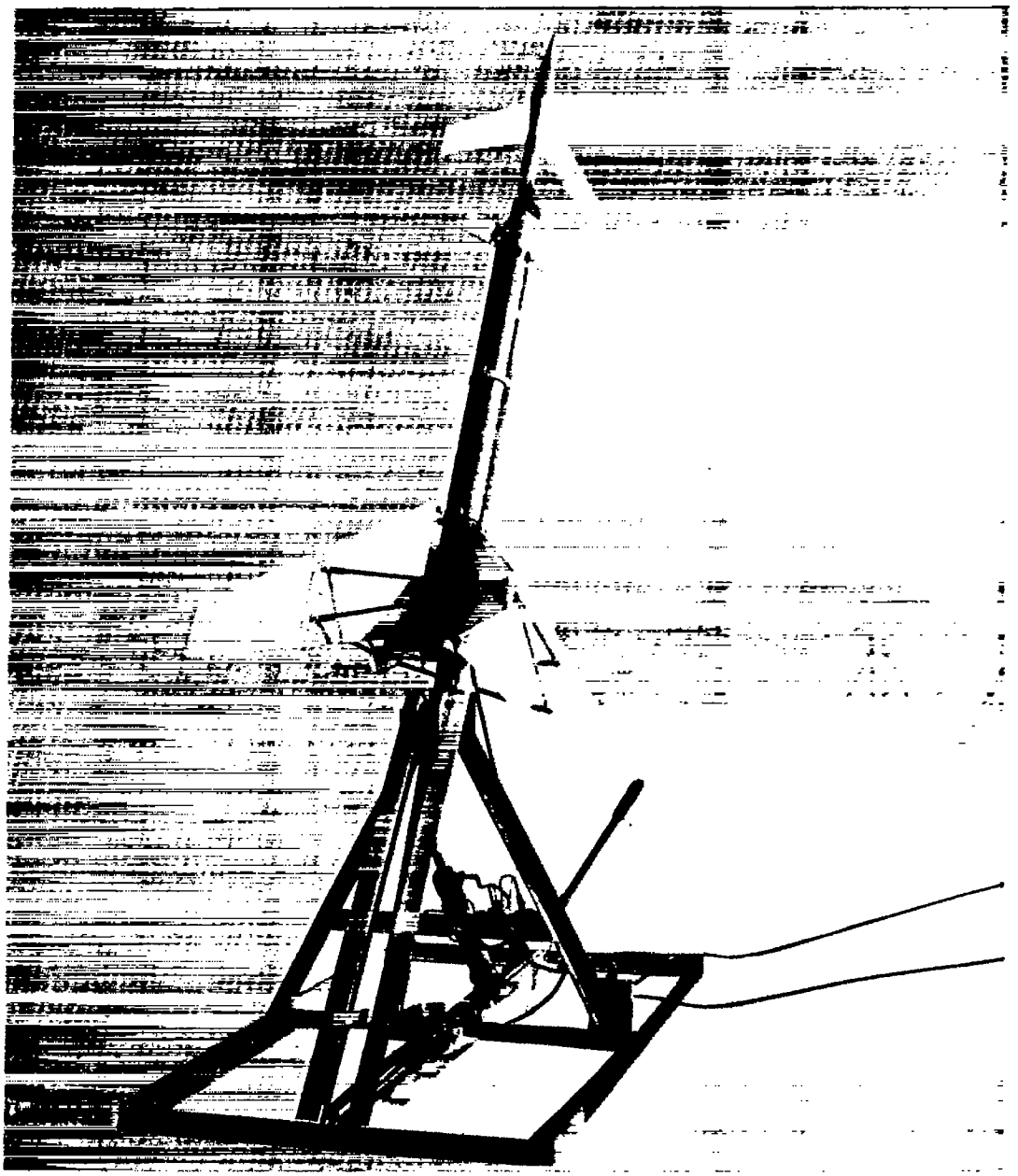

(e) Model and booster on rail launcher. L-92556.1

Figure 4.- Concluded.

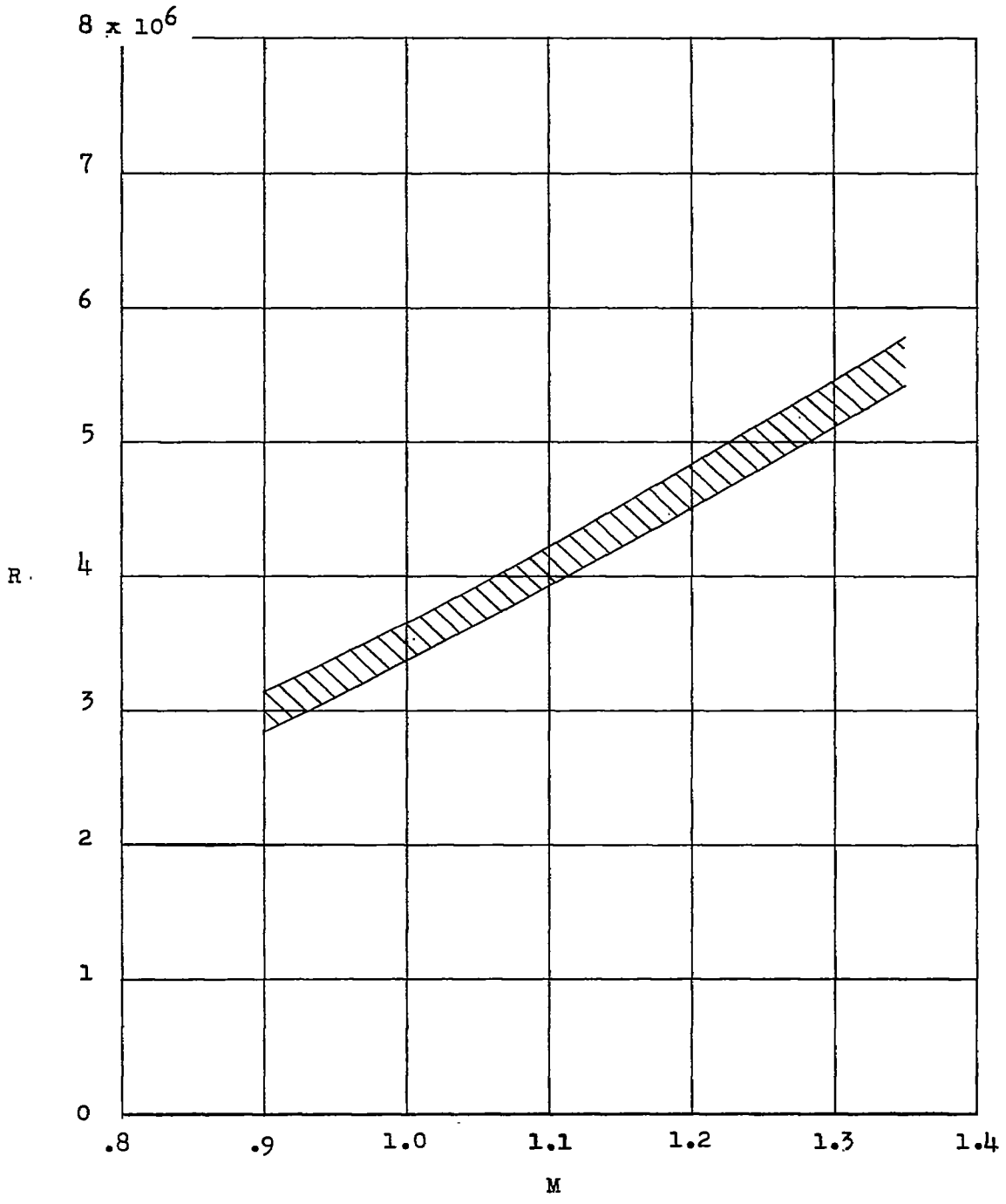

Figure 5.- Variation of Reynolds number with Mach number for models tested. Reynolds number is based on wing mean aerodynamic chord.

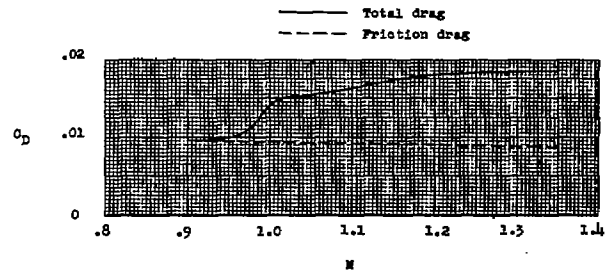

(a) Model A; basic configuration.

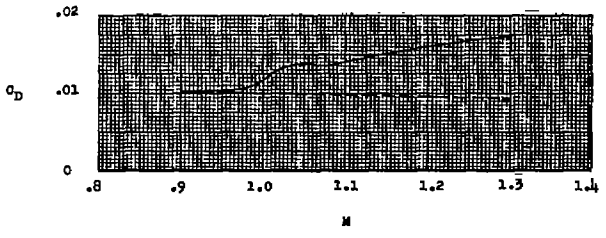

(b) Model B; M = 1.0 indentation.

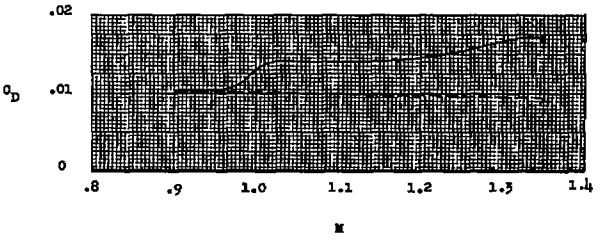

(c) Model C; M = 1.2 indentation.

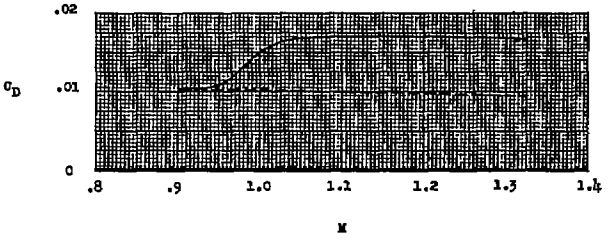

(d) Model D; M = 1.41 indentation.

Figure 6.- Variations of total drag coefficient and friction drag coefficient with Mach number.

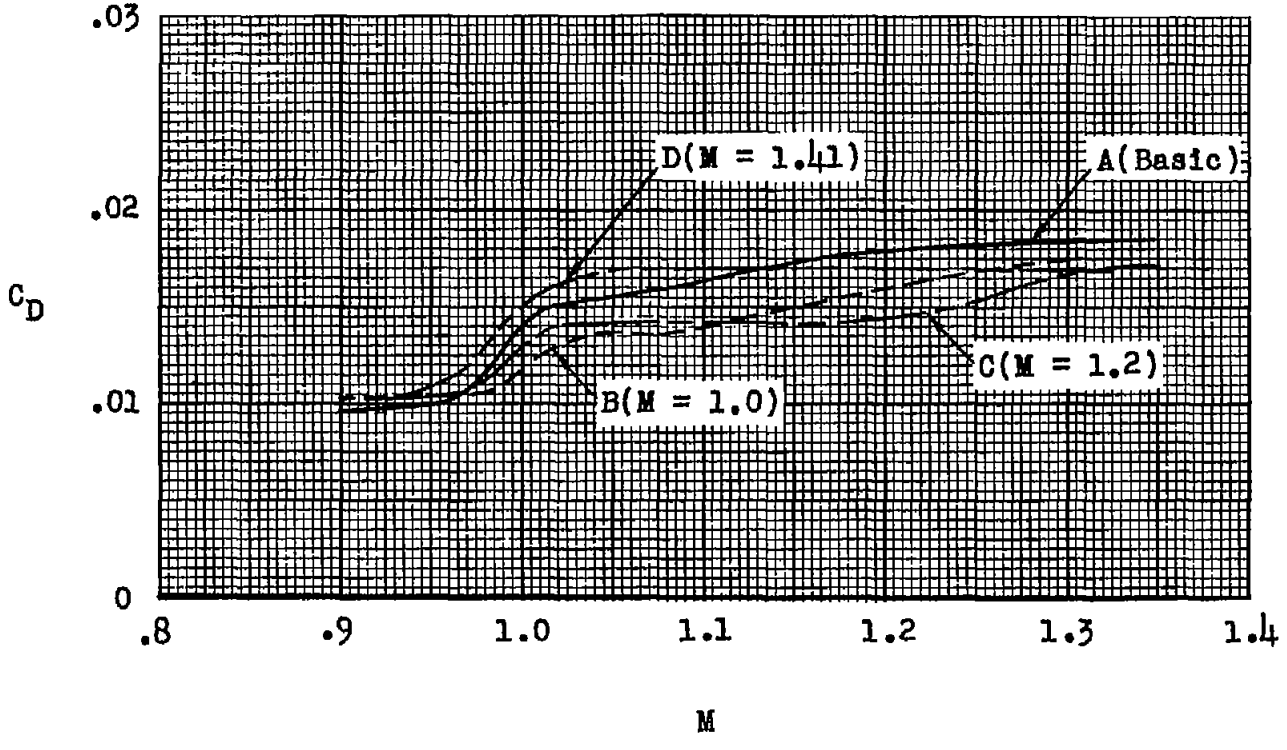

Figure 7.- Comparison of total drag coefficients for models tested.

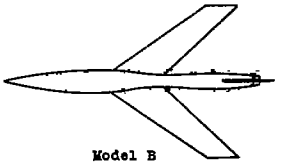

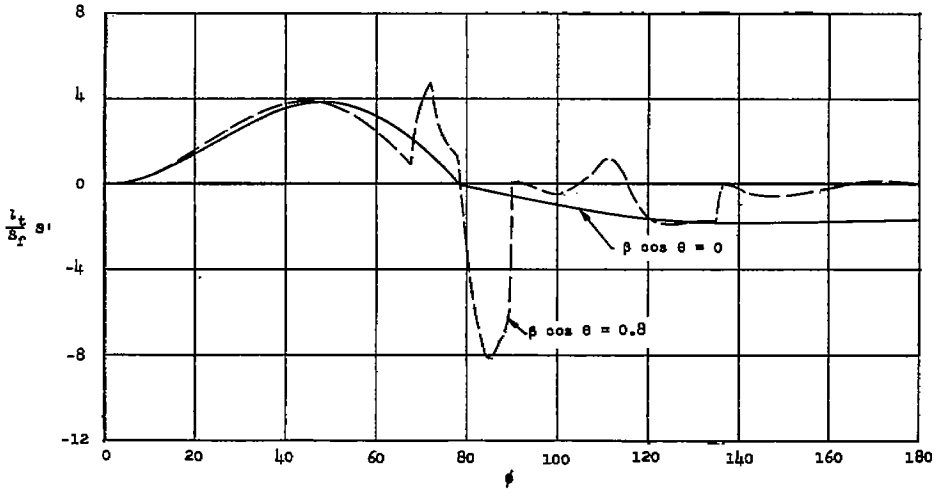

(a) Slope of area distribution for two values of $\beta \cos \theta$.

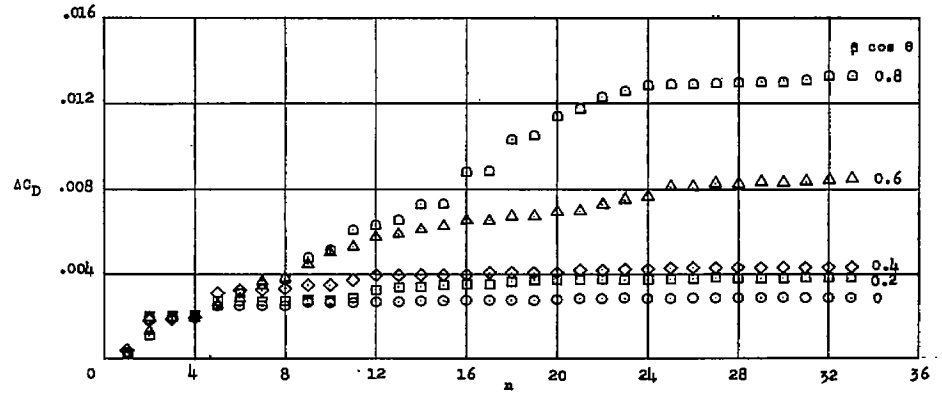

(b) Fourier series solution for several values of $\beta \cos \theta$.

Figure 8.- Examples of the area distribution slope curve and Fourier series solution for several values of $\beta \cos \theta$. Configuration with M = 1.0 indentation (model B).

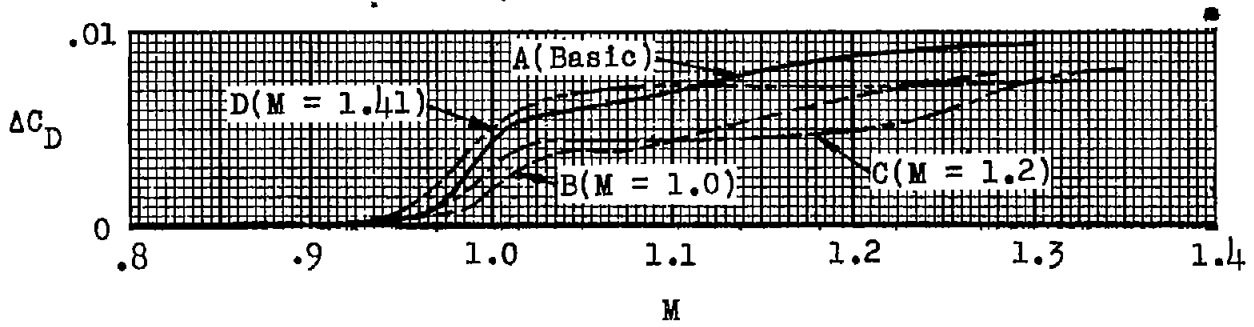

(a) Experimental pressure drags.

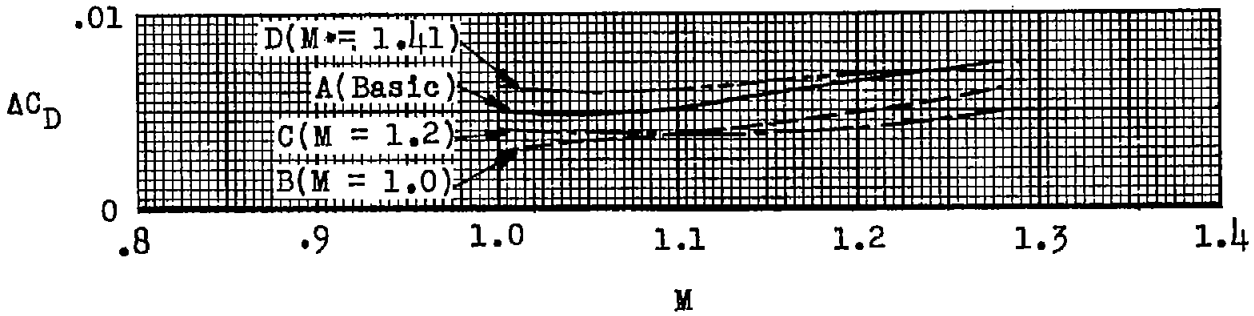

(b) Theoretical pressure drags.

Figure 9.- Comparisons of the experimental pressure drags and the theoretical pressure drags for the models tested.

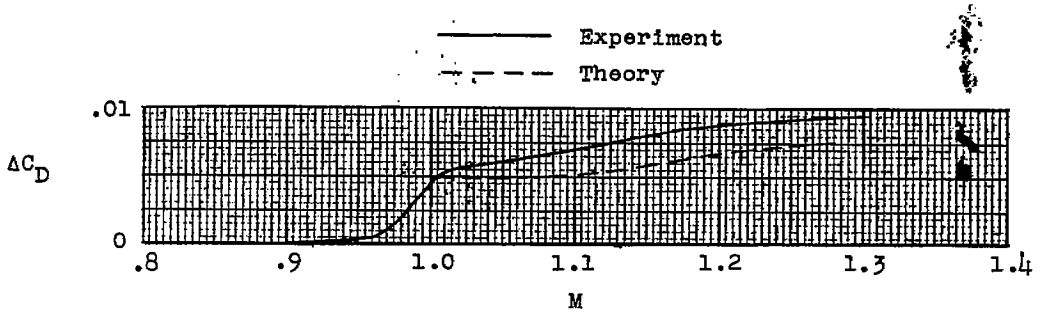

(a) Model A; basic configuration.

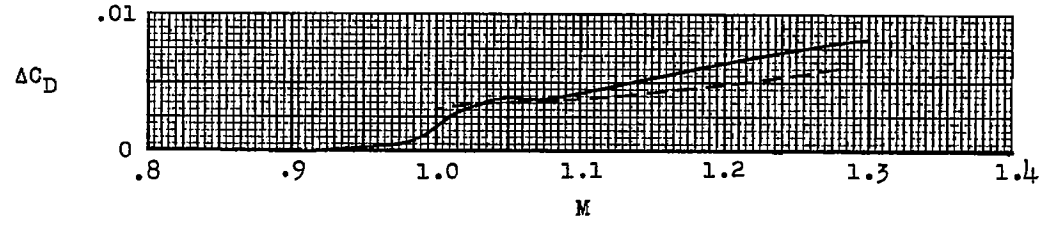

(b) Model B; M = 1.0 indentation.

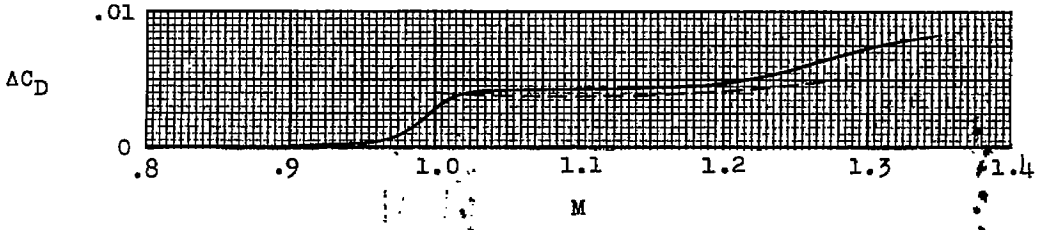

(c) Model C; M = 1.2 indentation.

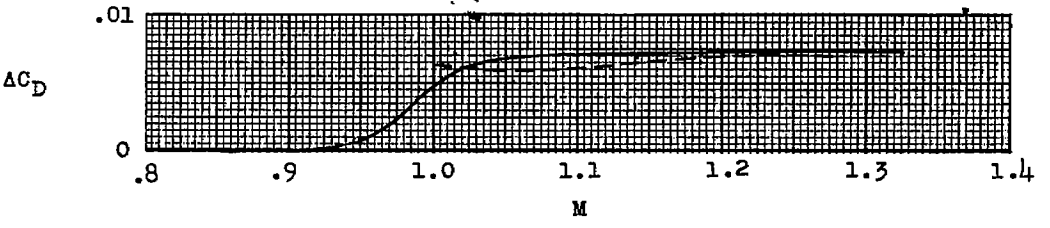

(d) Model D; M = 1.41 indentation.

Figure 10.- Comparisons of the theoretical pressure drags with the experimental pressure drags for each model tested.